J. Water Environ. Nanotechnol., 8(1): 52-65 Winter 2023

ORIGINAL RESEARCH PAPER

Visible light mediated photocatalytic anionic and cationic dyes degradation using ZnO-Fe_2O_3 nanocomposite

Armin Ehsani Amoli [1], Mojtaba Masoumi [1,*], Mazyar Sharifzadeh Baei [1], Fatemeh Babaei [2], Ghasem Firouzzade Pasha [3]

[1] Department of Chemical Engineering, Ayatollah Amoli Branch, Islamic Azad University, Amol, Iran
[2] Research and Development Center, Mazandaran Gas Company, Sari, Iran
[3] Department of Organic Chemistry, Faculty of Chemistry, University of Mazandaran, Babolsar, Iran

Received: 2022-11-03 Accepted: 2023-01-02 Published: 2023-02-12

ABSTRACT

In this work, hydrothermal technique and precursor materials obtained from the wastes of the filtration unit of the gas pressure reduction station were used to create a ZnO-Fe_2O_3 nanocomposite. FT-IR, FE-SEM, XRD, and TEM analyzes were used to investigate the properties of the produced nanocomposite. XRD analysis showed the structure of ZnO and Fe_2O_3 without impurities. The crystal size of the ZnO-Fe_2O_3 nanocomposite was determined to be about 53 nm. FE-SEM images showed a nanocomposite pattern with an approximate diameter of 50 nm. Finally, the visual decomposition of anionic and cationic dyes under visible light was used to study the photocatalytic activity of the ZnO-Fe_2O_3 nanocomposite. By exposing a metal halide lamp to light and darkness for 60 minutes and 150 minutes, respectively, it was possible to study the photocatalytic activity of the synthesized nanocomposite in removing anionic and cationic dyes from an aqueous medium. In the photocatalytic degradation of anionic and cationic dyes, the following factors were considered essential variables: pH, initial dye concentration, nanocomposite content, and exposure time. In this study, the degradation percentage of anionic and cationic dyes of ZnO-Fe_2O_3 nanocomposite with a ratio of 0.75:1 was 99.89 and 99.9%, respectively. The amount of band gap was calculated by the Tack plot method and electrical conductivity was calculated using electrochemical impedance spectroscopy, which reduced the band gap. And the resistance increases. Due to the acceleration of charge transfer at the heterogeneous junction surface and the suppression of electron/hole pairs from recombination, the ZnO-Fe_2O_3 nanocomposite significantly increased the visible light current response.

Keywords: Direct Blue anionic dye, Basic Yellow cationic dye, Visible light, Photocurrent, ZnO-Fe2O3 nanocomposite

How to cite this article
Amoli A. E., Masoumi M., Sharifzadeh Baei M., Babaei F., Firouzzade Pasha G., Visible light mediated photocatalytic anionic and cationic dyes degradation using ZnO-Fe2O3 nanocomposite. J. Water Environ. Nanotechnol., 2023; 8(1): 52-65
DOI: 10.22090/jwent.2023.08.006

INTRODUCTION

One of the most significant issues facing the globe now is water pollution [1]. One of the main global causes of disease and mortality is this problem. Various contaminants are present in both surface water and groundwater [2, 3]. Unpleasant tastes and odors in the water are signs that there are pollutants present. Different approaches have been thought to address pollutants depending on their source characteristics [4]. Organic matter, minerals, and physical components are the three categories into which water contaminants are categorized in terms of their nature [5-7]. Detergents and food industry effluents are two major organic water contaminants [8-10]. Colors [11], medicines [12], petroleum products [13], ammonia [14], chemical fertilizers [15], heavy metals [16], plant and tree vegetation [17], volatile organic matter [18], plant and tree foliage and volatile organic matter [19].

* Corresponding Author Email: *momasoomi88@gmail.com*

Turbidity in water is caused by mineral pollutants, which may occasionally be observed as suspended particles in the water [17-19]. Physical pollution of water resources also includes abrupt changes in the temperature and acidity of water supplies caused by human activity. Viruses, bacteria, and parasites are examples of contaminants with biological roots[20]. Many businesses, including the textile [21], rubber [22], and cosmetics [23] sectors, employ dyes extensively. Over 12,000 many forms of dyes are used in industry, and hundreds of tonnes are produced worldwide each year [24]. In addition to giving off a disagreeable look, the majority of these dyes in nature also impair light penetration, decrease photosynthetic activity, and impede biological development. Additionally, the majority of these colors are harmful and cancer-causing. Only 2% of all manufactured commercial colors are released directly into effluents [25] Therefore, before releasing wastewater into the environment, the dyes must be removed [26] Nowadays, heterogeneous photocatalytic techniques frequently employ semiconductors as catalysts [27]. With an energy gap of 3.2 electron volts and an excitation energy of 60 meV, zinc oxide (ZnO) nanoparticles may be stimulated by UV light in the 200–400 nm range [28], even in visible light's appearance [29]. Maximum absorption is seen in this material in the 385–360 nm wavelength region. Oxidized nanostructures are used in a variety of products, Burn ointments, sunscreen, screens, rubber, fire extinguishers, extinguishers, pigments for dye preparation, actuators, nanogenerators, sensors, transistors, diodes, coatings, solar cell electrodes, sequential DNA detectors Contrarily, catalytic nanoparticles are insoluble in the reaction fluid and are simple to separate [30] because of their greater dimensions than catalytic particles that are homogeneous. The nanocatalysts serve as a conduit for homogeneous and heterogeneous catalysts due to their highly active surface and capacity to be separated after the reaction [31-33] Nanotechnology decreases the quantity of catalyst, energy, and time needed to complete a process. Complete the response., the complexity and expense of making some nanocatalysts can be disregarded [34].

Iron oxide (Fe_2O_3), on the other hand, is appropriate for absorbing wavelengths in the visible light spectrum and has a relatively small energy gap [35]. The most significant magnetic benefit of Fe_2O_3 is the ease with which magnetic iron oxide may be readily extracted from solutions using an external magnetic field. Understanding the fundamental features of Fe_2O_3 is crucial to determine the photoelectric and photochemical properties because different semiconductors have sufficient energy gaps to catalyze a variety of chemical processes [36, 37]. Due to their chemical, magnetic, and photoluminescent capabilities, as well as their application as active components in gas sensors, ZnO and Fe_2O_3 have been proposed as luminescence cells in composite particles made of magnetic nuclei. Potential biological and biomedical uses for these composite particles include the detection of cancer cells, germs, and viruses, as well as magnetic isolation. In most of the research related to the photocatalytic degradation of Direct Blue 199 and Basic Yellow 28 dyes, ultraviolet light has been used as a source of radiation. Ultraviolet light is extremely dangerous for human skin and has a higher economic cost than visible light. Therefore, one of the innovations of this research is the synthesis of photocatalysts with the ability to act against visible light radiation. Also, the supply of raw materials in the photocatalyst synthesis process is from the waste of the filtration unit of the gas pressure reduction station, among other innovations used in this research. With this strategy, the waste cycle of a unit has become a photocatalytic product that can remove environmental pollution. In the following, the comparison of the degradation rate of colors using other photocatalysts along with photocatalyst characteristics and test conditions is presented in Table 1.

EXPERIMENTAL

Materials

Zinc acetate $Zn(CH_3COO)_2$, ethanol (CH_2COOH), hydrochloric acid (HCl), $6H_2O$. $FeCl_3$ and $4H_2O.FeCl_2$ was acquired from Merck Co for ZnO production, and deionized water was utilized to prepare solutions.

Synthesis of ZnO

The hydrothermal process was utilized to create ZnO. Using a magnetic stirrer, a particular amount of $Zn(CH3COO)_2$ was dissolved in distilled water, and a 0.5 M $Zn(CH3COO)_2$ solution was created. Then, 20cc of ethanol was added to the clear solution in a stainless steel autoclave with a Teflon wall. For 1 hour, samples were produced at 180 ° C. After that, the precipitate was separated using

Table 1. Comparison of research results with other studies

photocatalysts	Target Compound	Condition	Degradation Efficiency (%)	ref
Ce co-doped Ag–ZnO	NBB	solvothermal method 40 min solar light	90%	[38]
Ag-ZnO/TiO_2	MB/RhB/MG (5 mg/L)	Hydrothermal method time 120 min Xenon lamp(300 W)	99% (MB) 87%(RhB) 71%(MG)	[39]
Au-ZnO/TiO_2	MO (10 mg/L)	Hydrothermal method time 300 min Mercury lamp(300 W)	95%	[40]
In2O3/ZnO	RBB (50mg/L)	Sol-gel method time 120 min sun light	96%	[41]
PANI-ZnO	MB MG (3.2mg/L)	polymerization method time 180 min sunlight(300 W)	99%	[42]
AgBr-ZnO	MB (10 mg/L)	Hydrothermal method time 240 min LED	87%	[43]

a vacuum filter and washed numerous times with deionized water and ethanol to eliminate salt and other contaminants. Finally, it was dried for 4 hours at 70 ° C [44].

Synthesis of Fe_2O_3

To start the chemical production of Fe_2O_3 nanoparticles, a mixture of 0.46 mmol of $6H_2O$. $FeCl_3$ and 0.3 mmol of $4H_2O.FeCl_2$ was used. In this combination, 6H2O.FeCl3 is a mixture of waste from the filtration unit of the gas pressure reduction station with Hcl. A magnet was used to stir the solution in a non-oxidizing solution at about 60°C for 30 minutes with a stoichiometric ratio of Fe+2. Then 0.90 mL of NH3, 43% alkaline hydrolysis was added and another was stirred at 60°C. Water was poured onto the magnetic nanoparticles created by the magnet. The magnet was again used to collect the magnetite nanoparticles, which were then cleaned and dried at room temperature. After cooling to ambient temperature, the product was calcined at 500°C for 4 hours to completely transform the magnetite nanoparticles into hematite nanoparticles. After this, the nanoparticles were collected twice using a magnet and once with water. The extracts were washed and dried at room temperature [39].

Synthesis of ZnO-Fe_2O_3

ZnO-Fe_2O_3 nanocomposite was synthesized using a hydrothermal process similar to ZnO synthesis. Using a magnetic stirrer, a certain amount of $Zn(CH3COO)_2$ was dissolved in distilled water and a 0.5 M $Zn(CH3COO)_2$ solution was created. After that, 20 cc of ethanol together with Fe_2O_3 was added to the clear solution in a stainless

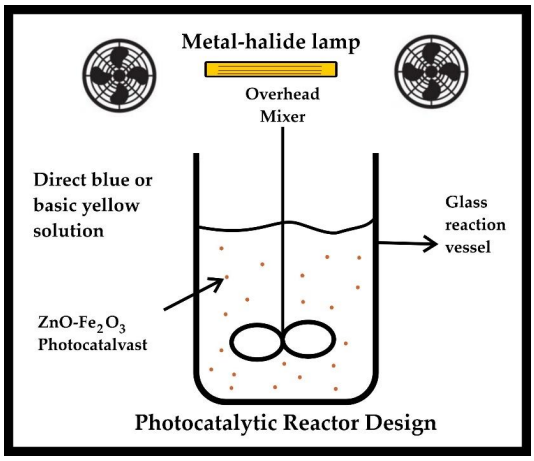

Fig.1 Photocatalytic reactor

steel autoclave. For 1 hour, samples were produced at 180°C. After autoclaving, the precipitate was separated using a vacuum filter and washed repeatedly with deionized water and ethanol to remove salt and other contaminants. Finally, it was dried for 4 hours at 70°C.

Characterization

For surface evaluation, FT-IR spectroscopy (Bruker tensor 27, Germany) was utilized in the frequency range of 400 to 4000 cm-1. The KBr pellet method was used to prepare the sample. The sample to KBr ratio in the synthesized materials was 1:100. In each example, 1 mg of dried material and 100 mg of KBr were homogenized in a transparent tablet at 200 kg/cm for 5 minutes using a mortar and pestle. Powder XRD in the 2-extent of 10-80 was performed on the synthesized materials using a Bruker d8 advanced XRD diffract meter (Cu K, = 1.5406). The surface morphology of the samples was studied using a field-emission scanning electron microscope (FE-SEM: Hitachi S-4160). Transmission electron microscopy has been used to examine basic and chemical resources at the nano-scale.

Photocatalytic test

The standard dye solution was generated at 90 mg/L, and the requisite concentrations were achieved by diluting the conventional remedy. The process of photocatalytic decomposition was then examined in terms of several experimental conditions, including pH (2–10), nanocomposite dosage (5-25 mg), dye concentration (10-90 mg/L), contact duration (60-240 min), and magnetic nanocomposite ratios. The visible light source was a 400 W Metal-halide lamp power noor company [45]. In a typical experiment, the pH of the produced dye solution was adjusted to the proper value, then the catalyst was added, and the combination was subjected to 60 minutes of darkness before being irradiated with a metal-halide lamp. At regular 20-minute intervals, 5 mL of each aliquot was collected. The schematic of the laboratory setup is shown in Fig.1.

$$removal(\%) = \left(\frac{C_0 - C_e}{C_0}\right) \times 100 \quad (1)$$

C_0 and C_e are the initial and residual concentrations at time t (min), respectively (mg/L).

Photoelectrochemical test

The electrochemical workstation Autolab PSGSTAT-204, Metrohm, Netherlands, was used for the photoelectrochemical studies, which included photocurrent and electrochemical impedance spectroscopy (EIS) measurements. As the reference and counter electrodes, Ag/AgCl and Pt wire electrodes were employed, respectively. The functioning electrodes were made in the following manner: 0.015 g of the prepared photocatalyst was combined with 0.005 g of PVDF and 60 l of N-methyl-2-pyrrolidone (NMP). 20 l of the slurry was deposited onto a 1 cm FTO glass electrode, and the electrodes were oven dried for a few hours. The excitation light source was a 400 W Metal Halide lamp. The electrolyte was 0.1 M Na_2SO_4 aqueous solution. Electrochemical impedance spectroscopy (EIS) measurements were carried out at an open circuit potential throughout a frequency range of 10 kHz to 100 mHz.

RESULTS AND DISCUSSION

FTIR

The FT-IR of the produced ZnO-Fe_2O_3 nanocomposite is shown in Fig.2. Peak 3431 cm^{-1} in this Fig is connected to O-H bonds. The presence of O-H peaks is critical for increasing photocatalytic activities. Under certain situations, OH groups create an electron and a hole, causing the electron to transfer and react with the pollutant's free radicals. The presence of CO_2 in the air causes the 2428 cm^{-1} peak. Peaks 892 cm^{-1} and 835 cm^{-1} show the production of a ZnO-Fe_2O_3 nanocomposite as well. Peaks 587 cm^{-1} and 444 cm^{-1} reflect the vibrational bonds Fe-O and Zn-O, respectively.[46]

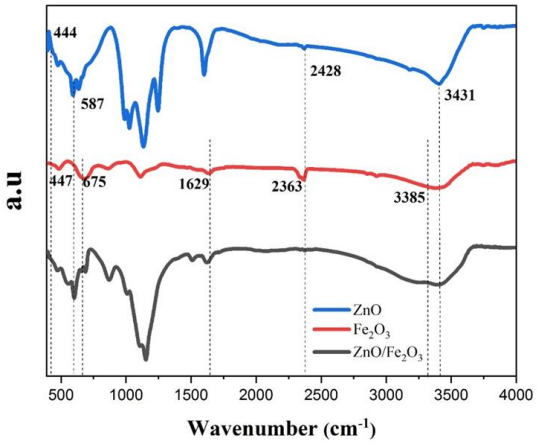

Fig.2. FT-IR Of nanoparticle and nanocomposite

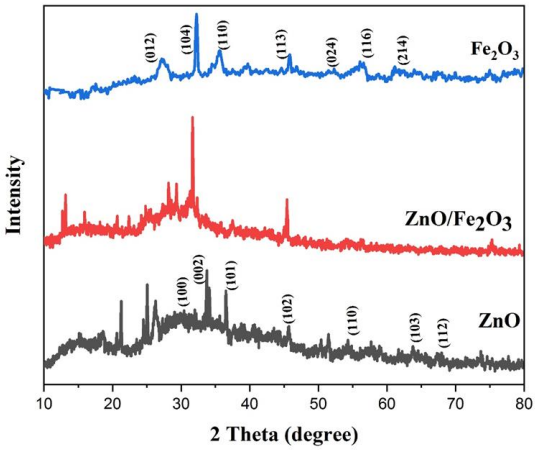

Fig. 3. XRD Of nanoparticle and nanocomposite

XRD

The XRD pattern of produced ZnO, Fe_2O_3 nanoparticles, and ZnO-Fe_2O_3 nanocomposite is shown in Fig.3. As can be seen, the XRD pattern for ZnO (card number 0072-024-00) and iron oxide (card number 1451-036-00) samples matches to their standard card, with no extra impurity-related peak identified. Diffraction peaks associated with pages (100), (002), (101), (102), (110), (103), (200), (112), (201), (004), (202) ZnO and diffraction peaks associated with plates (012), (104), (110), (006), (113), (202), (024), (116), (018), (214), (300) iron oxides are shown in Fig. 2, ZnO has a hexagonal crystal structure and has a lattice constant a = b = 3/3138, c = 3/2366, α = β = 33, and γ = 323 and Fe_2O_3 also has a hexagonal crystal structure and has a lattice constant α = β = 33, C = 35/992, a = b = 3/358 and γ = 323. The crystal size of the particles in the ZnO-Fe_2O_3 nanocomposite was determined using the Debay-Scherer relationship [47] and was found to be around 53 nm.

SEM AND TEM

Fig.4 (a) and (b) show SEM images related to ZnO nanoparticles and ZnO/Fe_2O_3 nanocomposite. As seen in Fig.3, the morphology of ZnO nanoparticles is flower-shaped, and each of these flower-like clumps consists of many nanometer-sized particles. In addition, the synthesized nanoparticles have good uniformity in particle size distribution. With the addition of iron oxide nanoparticles and the formation of the nanocomposite, the primary structure of nanoparticles is changed and the particles have a variety of sizes, and due to the nature of magnetic nanoparticles, they assume a lumpy state. Also, the proper coating of ZnO nanoparticles on iron oxide nanoparticles and the cluster structure of the nanocomposite after adding iron oxide nanoparticles are visible in TEM images Fig. 5(a,b)

Calibration

To begin research and extensive examinations of the hues of anionic and cationic dyes, calibration diagrams were created as seen in Fig.6. In the first step, the spectrophotometer was used to plot the spectrum of the dye solution with a concentration of 1-10 ppm in the range of 200-1100 nm, and it was discovered that anionic dye has an absorption peak at 319 wavelength - nanometer and cationic dye has an absorption peak at 510 wavelength - nanometer. In the second phase, color solutions with concentrations ranging from 1-100 ppm were generated, and their absorption was measured using a wavelength nanometer and a calibration diagram was created. The concentration of anionic and cationic dyes solution is determined using this diagram. As illustrated in the curve equation, by substituting solution adsorption for the amount y, the quantity x, which indicates the concentration of the solution, is calculated.

Band gap energy and DRS-UV

Photocatalytic dye degradation can take place under visible light because ZnO-Fe_2O_3 can easily absorb some of the visible light. This method includes dye excitation from the ground state (Dye) to the triplet excited state (Dye*) under visible light photons (> 400 nm). By injecting an electron into the conduction band of ZnO-Fe_2O_3, this excited

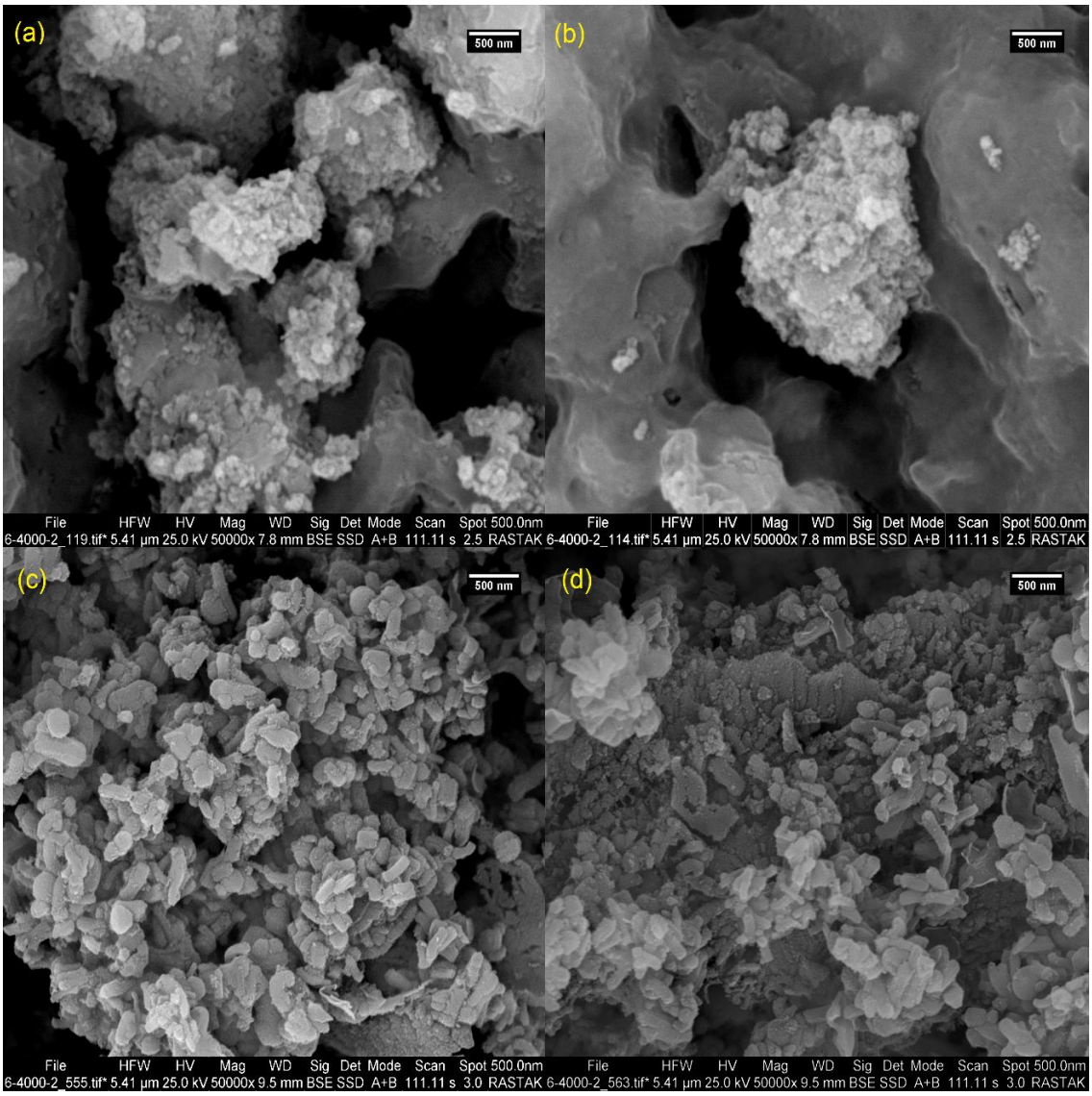

Fig. 4. (a,b) SEM of ZnO nanoparticle and (c,d)ZnO-Fe_2O_3 nanocomposite

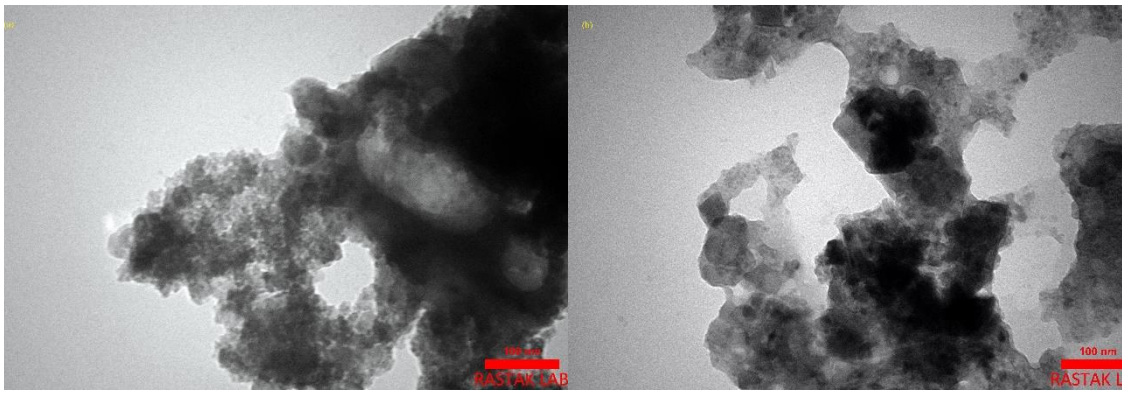

Fig. 5. (a,b)TEM of ZnO-Fe_2O_3 nanocomposite

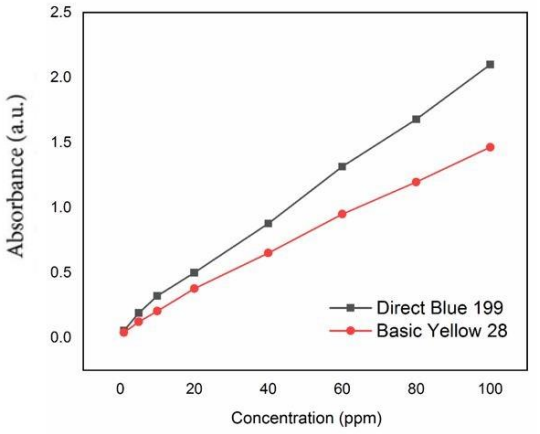

Fig. 6. Anionic and cationic dyes calibration curve

state dye species is further transformed into a semi-oxidized radical cation (Dye+). Superoxide radical anions (O_2) are produced as a result of an interaction between these trapped electrons and the dissolved oxygen in the system, which in turn causes the creation of hydroxyl radicals (OH). The organic molecules shown in Fig. 7 have been oxidized mostly by these OH radicals [48]. The results obtained from the diffuse reflectance spectroscopy (DRS) analysis are shown in Fig. 8(a). The band gap of nanocomposite was calculated using the following equation:

$$\alpha h\nu = A(h\nu - Eg)^{n/2} \quad (4)$$

The band gap related to the nanocomposite was calculated as 1.8, which indicates that the samples can absorb light with a wavelength in the range of 400-800 nm. Accordingly, all samples were active in the visible region. The photoluminescence (PL) method is one of the most common techniques for evaluating the photocatalytic properties of materials. In this regard, information about light quality, electron-hole (e-h) recombination, structural defects, and cracks can be obtained. As the intensity diminishes, the e-h recombination is mitigated. As shown in Fig. 8(b), the e-h recombination of the sample is acceptable and therefore, nanocomposite has the good photocatalytic activity

Photocatalytic degradation

A ZnO-Fe_2O_3 nanocomposite's behavior as a photocatalytic degrader of the colors produced by anionic and cationic dyes was investigated. In general, the presence of this nanocomposite allows a range of intermediates to be formed when anionic and cationic dyes are exposed to a metal halide lamp, all of which are ultimately transformed into CO_2, H_2O, and HCl, which are the end products. Just as these hydroxyl radicals are crucial in the oxidation of other organic compounds, HO hydroxyl radicals and O_2 anions are good oxidation agents for the colors of anionic and cationic dyes. The pH and photocatalytic architecture of the apparatus, among other factors, all affect how many of these organisms are present there

The influence of light

To determine the best period for the deterioration of the anionic and cationic dyes in the aquatic environment. Fig.9 and 10 depict experiments that were carried out under the same settings but at different periods. As a result, 90 minutes of darkness and 210 minutes of full light were considered. There was minimal change in eliminating anionic and cationic dyes throughout the 90 minutes of darkness. Because the adsorption and desorption processes are completed reasonably quickly in the first 60 minutes, the dark period of 60 minutes was taken into account. Up to 150 minutes, there was a very considerable shift in the duration of metal halide light irradiation, but after that, the fluctuations were nearly consistent. So, after 150 minutes of brightness, the degree of deterioration for ZnO-Fe_2O_3 nanocomposites in proportion 1: 075 was 92.66%, while the rate of deterioration for cationic dye for ZnO-Fe_2O_3 nanocomposite in proportion 1: 075 was 89.54%. In 180 minutes and 210 minutes, the percentage of degradation for anionic dye is 94.32% for ZnO-Fe_2O_3 nanocomposite with a ratio of 1: 075, and the proportion of deterioration for cationic dye is 90.67% and 91.12% for ZnO-Fe_2O_3 nanocomposite with a ratio of 1: 075. As a result, up to this dark stage, 60 minutes and 150 minutes of metal halide light irradiation might be regarded as the best moment to continue the experiments.

pH effect

The pH of the solution is an essential variable in photocatalytic reactions because it controls the surface charge of the semiconductor photocatalyst. The degradation of Direct Blue 199 color decreased with an increase in pH, which may be the reason for the misplaced adsorption of the product at high pH on the catalyst surface through electrostatic adsorption. To investigate the effect of pH, a solution of Direct Blue 199 and Basic Yellow dyes

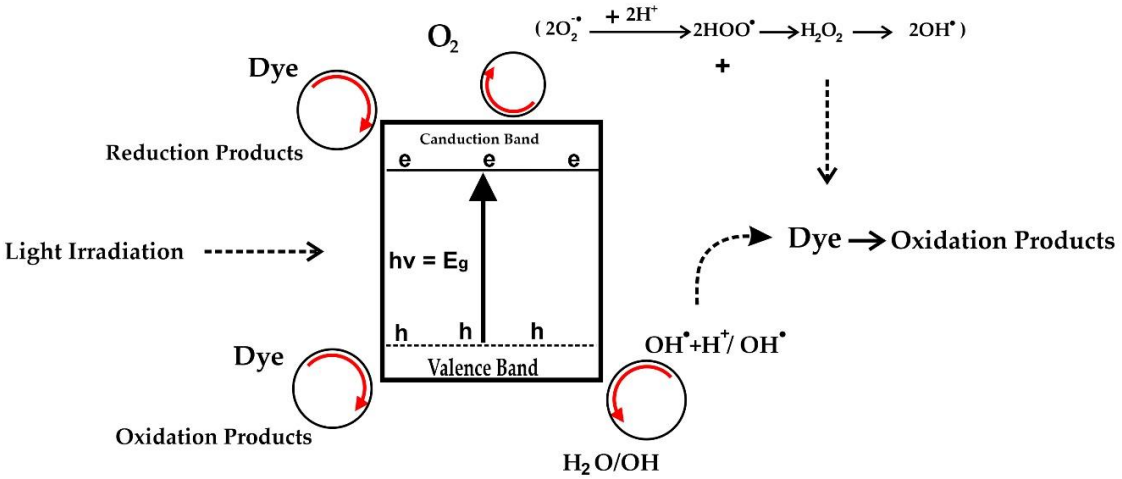

Fig. 7. Anionic and cationic dyes calibration curve

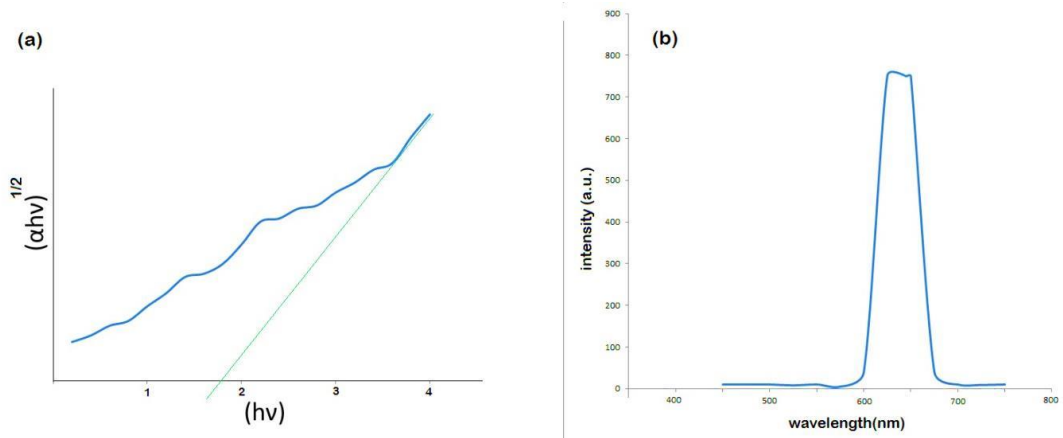

Fig. 8. a) UV- vis DRS spectra and b)PL analysis of Nanocomposite

with a concentration of 50 mg/liter was prepared and with the help of a pH meter, the pH was adjusted to 3 and 5 with the help of HCl and the pH was adjusted to 9 and 11 with the help of NaOH. and in 60 minutes of darkness and 180 minutes of light, the amount of degradation of Direct Blue 199 and Basic Yellow colors was measured in the presence of a metal halide lamp, and based on the results obtained (Fig.10 and 11), which is also shown in Fig. 9, the highest amount of degradation Direct Blue 199 color was obtained from aqueous solution at pH=2 equal to 98.21 and the maximum degradation value of Basic Yellow color was obtained from aqueous solution at pH=10 equal to 98.88 and this pH was selected as optimal pH in the continuation of the research (Fig.11).

Effect of photocatalyst dosage

The impact of photocatalyst amount was looked into by adding 5, 10, 20, 15, and 25 mg of ZnO-Fe_2O_3 nanocomposite, and the result demonstrated that increasing the mass to 15 mg increased degradation efficiency, and the continuous result demonstrated occurred. The reason for this is that as the amount of catalyst grows, so does the number of active sites, increasing the degrading efficiency. However, increasing the quantity of the catalyst raises the turbidity of the solution, lowering visible light penetration and preventing light from reaching and exciting the catalyst surface. As well as water excitation and hydroxyl radical formation as a result, the catalyst deteriorates, resulting in

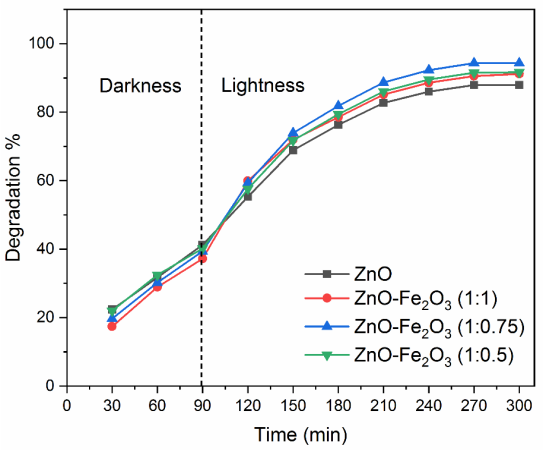

Fig. 9. Degradation and the Effect of Photocatalytic Value At pH 7, the starting anionic dye solution concentration was 50 ppm, the dye solution temperature was 25 ° C, and the adsorbent was 12 mg.

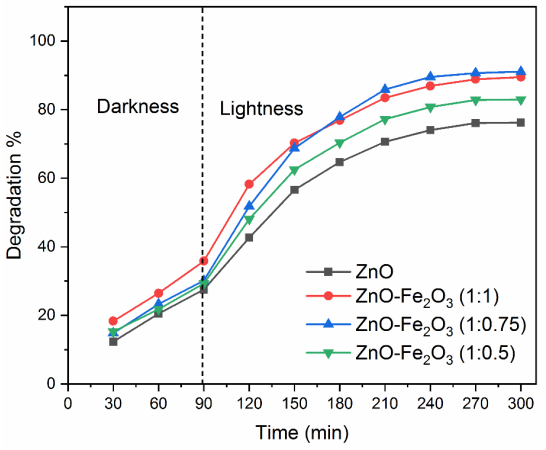

Fig. 10. Influence of Light and Darkness on Penetration Efficiency of cationic dyes, pH: 7, Initial Concentration of Dye Solution: 50 ppm, Temperature of Dye Solution: 25°C, Absorbance: 12 mg

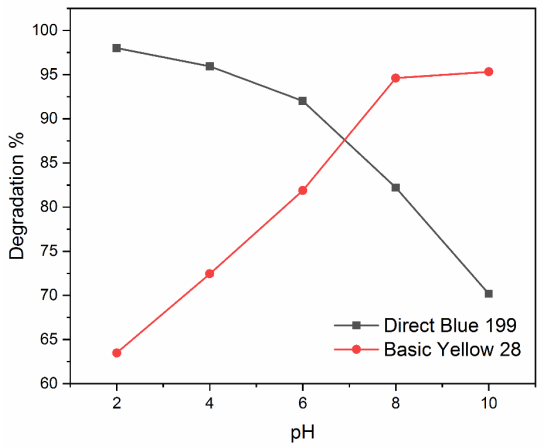

Fig. 11. Influence of pH on Decomposition Efficiency of anionic and cationic dyes, starting dye solution concentration: 50ppm, dye solution temperature: 25 C, absorbent value: 15mg, and length of darkness 60 minutes and brightness 150 minutes.

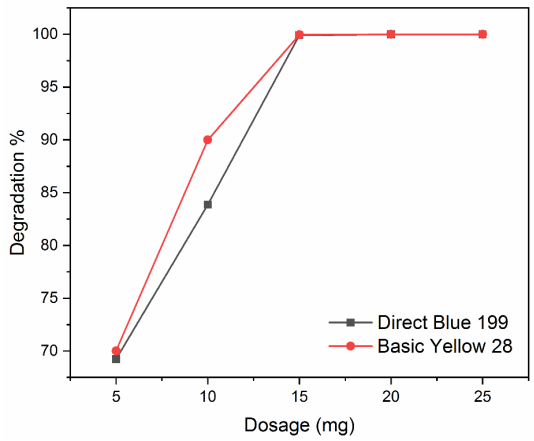

Fig. 12. Influence of photocatalyst cost on the degradation performance of anionic and cationic dyes, pH: 7 Initial concentration of dye solution: 50 ppm, dye solution temperature: 25 ° C and duration of darkness 60 minutes and brightness 150 minutes

lower efficiency. Fig.12 depicts the findings of an investigation into the influence of a ZnO-Fe_2O_3 nanocomposite photocatalyst on the deterioration effect of anionic and cationic dyes.

Effect of initial concentration

The influence of the starting concentration of anionic and cationic dyes on photocatalytic degradation performance was examined using nanocatalysts with varying dye concentrations (20, 40, 60, 80, and 100 mg/L). Fig.13 demonstrates that increasing the concentration of anionic and cationic dyes from 20 to 100 mg/L reduces degradation efficiency, which might be attributed to the saturation of the active sites in the adsorbent and lower light penetration. To limit the degradation of anionic and cationic dyes in the solution at greater concentrations, a concentration of 60 mg/L was deemed the best concentration of anionic and cationic dyes for this investigation. This dye's photocatalytic breakdown is nearly complete at its initial concentration.

Temperature effect

Temperature effects on photocatalytic degradation of anionic and cationic dyes hues were studied at three different temperatures:

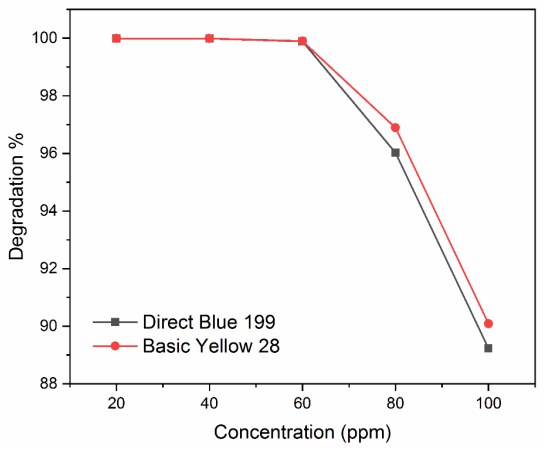

Fig. 13. Influence of preliminary awareness on degradation performance of anionic and cationic dyes, pH = 2, 10, dye solution temperature: 25 ° C, absorbent value: 15mg and duration of darkness 60 minutes and brightness 150 minutes

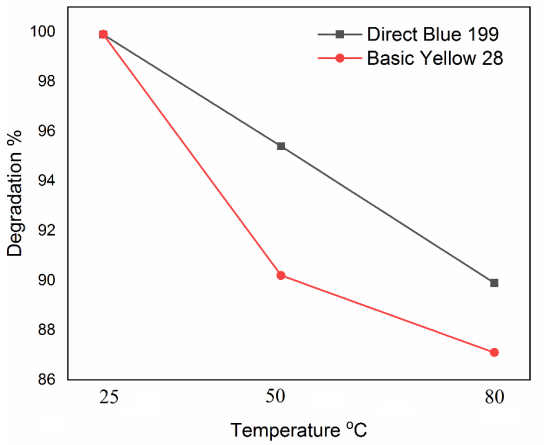

Fig. 14. Temperature Influence on decomposition efficiency of anionic and cationic dyes

25, 50, and 80 ° C. The data showed that the degradation efficiency of anionic and cationic dyes reduced with rising temperature, as shown in Fig.14, total deterioration at standard temperature happened 40 minutes faster than at other temperatures. It helps to improve the efficiency of this photocatalyst in the degradation process. As a result, the ideal in this experiment, the temperature was 25 degrees Celsius.

Catalyst recovery

Based on the best circumstances that resulted in a complete breakdown of anionic and cationic chemical dyes in 150 minutes of light following the degradation process in the first sample, the solution was developed to assess if ZnO-Fe_2O_3 nanocomposite may be reused after photocatalytic removal. A new dye of anionic and cationic dyes was prepared, and the percentage of degradation was recalculated in 150 minutes with the same optimal conditions. This process was repeated up to five times with the same nanocomposite, and the recovery percentage of this nanoparticle was up to five hours. The findings were computed and are shown in Fig.15.

Photoelectrochemical evaluation

The photocurrent transient response is an effective tool for assessing the photoresponse of composite photocatalysts. The chronoamperogram of ZnO and ZnO-Fe_2O_3 electrodes is shown in Fig.16. Photocurrents were more significant in the ZnO-Fe_2O_3 electrode than in the ZnO electrode. The smaller band gap of the ZnO-Fe_2O_3 nanocomposite led to increased visible light absorption, resulting in higher photocurrent [49]. Because of the presence of Fe_2O_3 in this electrode, this rise suggested the highest photo electrocatalytic activity, i.e., maximal charge transfer and minimal charge carrier recombination [50-52].

EIS analysis was used to assess the charge transfer resistance and separation efficiency of photogenerated electrons [52]. The EIS spectrum's impedance arc radius represents the interface layer resistance at the electrode surface, and the smaller the impedance arc radius, the better the charge transfer efficiency (Fig.17). The impedance arc radius of ZnO-Fe_2O_3 in radiation settings is less than that of ZnO in both dark and radiation settings, indicating that the ZnO-Fe_2O_3 electrode has less electrochemical resistance and more intense interfacial charge transfer than the ZnO electrode. The decrease in the band gap in the ZnO-Fe_2O_3 electrode (as compared to the ZnO electrode) increased the charge carriers at the photocatalyst surface (during light irradiation). The addition of Fe_2O_3 reduced the band gap of the ZnO band structure, which increased the charge Transfer efficiency on the ZnO-Fe_2O_3 electrode surface during photoelectrochemical processes [28, 29, 53].

CONCLUSION

Industrial effluent pollution of water resources has resulted in several environmental challenges in modern civilization. Pollutants in industrial effluents include organic molecules that are colored, such as

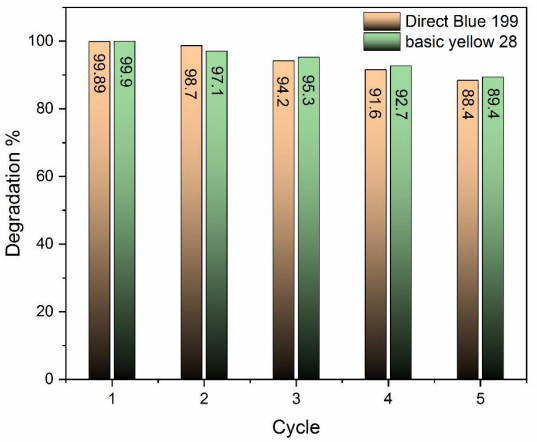

Fig. 15. Recovery percentage of ZnO-Fe_2O_3 nanocomposite

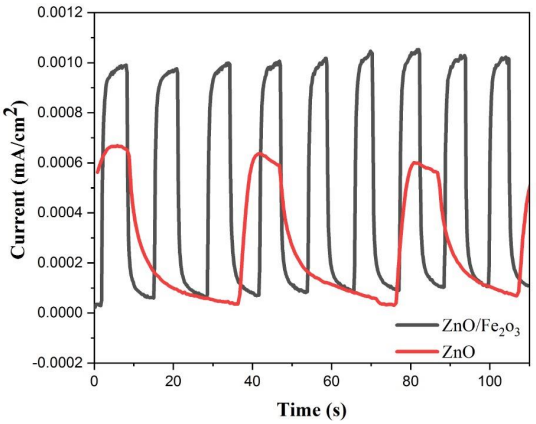

Fig. 16. Photocurrent responses of ZnO and ZnO-Fe_2O_3 nanocomposite profiles

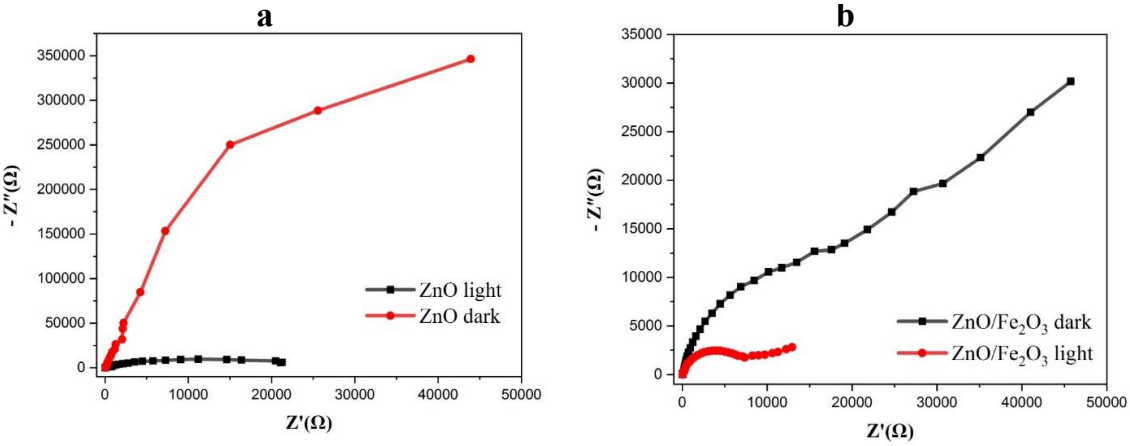

Fig. 17. Representation of the EIS results for the ZnO (a) and ZnO-Fe_2O_3 (b) under dark and light conditions.

anionic and cationic dyes. Their presence in water inhibits sunlight from penetrating the depths of rivers, disrupting photosynthesis, and on the other hand stimulates the fast development of particular forms of algae, reducing water-soluble oxygen and preventing light from reaching aquatic organisms. In this work, a simple hydrothermal approach was used to create a ZnO-Fe_2O_3 nanocomposite, and The nanocomposite's morphological and structural characteristics were investigated using XRD, FE-SEM, and FT-IR methods. The photocatalytic activity of the synthesized nanocomposite in eliminating the hues of anionic and cationic dyes from an aqueous medium was studied by irradiating a metal halide lamp for 60 minutes of darkness and 150 minutes of light. The influence of pH, catalyst dosage, dye concentration, and temperature on the molecular breakdown of anionic and cationic dyes was studied. The findings demonstrated full photocatalytic destruction of anionic dye in acidic circumstances pH = 2 and 25 ° C with a dosage of 15 mg, as well as photocatalytic degradation of cationic dye in game conditions pH = 10 and 25 ° C with a dose of 15 mg. of nanocatalyst (15 mg) The benefits of this nanocomposite in the process of degradation of anionic and cationic dyes molecules include its good photocatalytic action, high stability, and low dosage. Experiment findings indicated that the ZnO-Fe_2O_3 nanocomposite has a substantial ability to degrade the anionic and cationic dyes from aqueous solution, and its usage in the treatment of effluents containing this dye is suggested.

CONFLICT OF INTEREST

The authors declare no conflict of interest.

REFERENCES

[1] Bullen, J.C., H.F. Heiba, A. Kafizas, and D.J. Weiss, 2022. Parasitic light absorption, rate laws and heterojunctions in

the photocatalytic oxidation of arsenic (III) using composite TiO2/Fe2O3. Chemistry-A European Journal.

[2] Saha, N., M.S. Rahman, M.B. Ahmed, J.L. Zhou, H.H. Ngo, and W. Guo, 2017. Industrial metal pollution in water and probabilistic assessment of human health risk. Journal of environmental management, 185: 70-78. https://doi.org/10.1016/j.jenvman.2016.10.023

[3] Andrade, L., J. O'Dwyer, E. O'Neill, and P. Hynds, 2018. Surface water flooding, groundwater contamination, and enteric disease in developed countries: A scoping review of connections and consequences. Environmental pollution, 236: 540-549. https://doi.org/10.1016/j.envpol.2018.01.104

[4] Ali, I., X. Mbianda, A. Burakov, E. Galunin, I. Burakova, E. Mkrtchyan, A. Tkachev, and V. Grachev, 2019. Graphene based adsorbents for remediation of noxious pollutants from wastewater. Environment international, 127: 160-180. https://doi.org/10.1016/j.envint.2019.03.029

[5] Lehmann, J. and M. Kleber, 2015. The contentious nature of soil organic matter. Nature, 528(7580): 60-68. https://doi.org/10.1038/nature16069

[6] Cotrufo, M.F., J.L. Soong, A.J. Horton, E.E. Campbell, M.L. Haddix, D.H. Wall, and W.J. Parton, 2015. Formation of soil organic matter via biochemical and physical pathways of litter mass loss. Nature Geoscience, 8(10): 776-779. https://doi.org/10.1038/ngeo2520

[7] Sillanpää, M., M.C. Ncibi, A. Matilainen, and M. Vepsäläinen, 2018. Removal of natural organic matter in drinking water treatment by coagulation: A comprehensive review. Chemosphere, 190: 54-71. https://doi.org/10.1016/j.chemosphere.2017.09.113

[8] Kundu, S., M.V. Coumar, S. Rajendiran, A. Rao, and A.S. Rao, 2015. Phosphates from detergents and eutrophication of surface water ecosystem in India. Current science: 1320-1325.

[9] Martínez-Huitle, C.A., M.A. Rodrigo, I. Sirés, and O. Scialdone, 2015. Single and coupled electrochemical processes and reactors for the abatement of organic water pollutants: a critical review. Chemical reviews, 115(24): 13362-13407. https://doi.org/10.1021/acs.chemrev.5b00361

[10] Ravindran, R. and A.K. Jaiswal, 2016. Exploitation of food industry waste for high-value products. Trends in biotechnology, 34(1): 58-69. https://doi.org/10.1016/j.tibtech.2015.10.008

[11] Irfan, M., T. Butt, N. Imtiaz, N. Abbas, R.A. Khan, and A. Shafique, 2017. The removal of COD, TSS and colour of black liquor by coagulation-flocculation process at optimized pH, settling and dosing rate. Arabian Journal of Chemistry, 10: S2307-S2318. https://doi.org/10.1016/j.arabjc.2013.08.007

[12] Udaiyappan, A.F.M., H.A. Hasan, M.S. Takriff, and S.R.S. Abdullah, 2017. A review of the potentials, challenges and current status of microalgae biomass applications in industrial wastewater treatment. Journal of Water Process Engineering, 20: 8-21. https://doi.org/10.1016/j.jwpe.2017.09.006

[13] Nguyen, P.M., M. Afzal, I. Ullah, N. Shahid, M. Baqar, and M. Arslan, 2019. Removal of pharmaceuticals and personal care products using constructed wetlands: effective plant-bacteria synergism may enhance degradation efficiency. Environmental Science and Pollution Research, 26(21): 21109-21126. https://doi.org/10.1007/s11356-019-05320-w

[14] Gurdeep, K. and M.S. Reddy, 2015. Effects of phosphate-solubilizing bacteria, rock phosphate and chemical fertilizers on maize-wheat cropping cycle and economics. Pedosphere, 25(3): 428-437. https://doi.org/10.1016/S1002-0160(15)30010-2

[15] Kim, I., J. Yun, T. Badloe, H. Park, T. Seo, Y. Yang, J. Kim, Y. Chung, and J. Rho, 2020. Structural color switching with a doped indium-gallium-zinc-oxide semiconductor. Photonics Research, 8(9): 1409-1415. https://doi.org/10.1364/PRJ.395749

[16] Panchal, P., D.R. Paul, A. Sharma, D. Hooda, R. Yadav, P. Meena, and S. Nehra, 2019. Phytoextract mediated ZnO/MgO nanocomposites for photocatalytic and antibacterial activities. Journal of Photochemistry and Photobiology A: Chemistry, 385: 112049. https://doi.org/10.1016/j.jphotochem.2019.112049

[17] Rügner, H., M. Schwientek, M. Egner, and P. Grathwohl, 2014. Monitoring of event-based mobilization of hydrophobic pollutants in rivers: Calibration of turbidity as a proxy for particle facilitated transport in field and laboratory. Science of the Total Environment, 490: 191-198. https://doi.org/10.1016/j.scitotenv.2014.04.110

[18] Nasrabadi, T., H. Ruegner, Z.Z. Sirdari, M. Schwientek, and P. Grathwohl, 2016. Using total suspended solids (TSS) and turbidity as proxies for evaluation of metal transport in river water. Applied Geochemistry, 68: 1-9. https://doi.org/10.1016/j.apgeochem.2016.03.003

[19] Mativenga, P.T. and A. Marnewick, 2018. Water quality in a mining and water-stressed region. Journal of cleaner production, 171: 446-456. https://doi.org/10.1016/j.jclepro.2017.10.030

[20] Bukola, D., A. Zaid, E.I. Olalekan, and A. Falilu, 2015. Consequences of anthropogenic activities on fish and the aquatic environment. Poultry, Fisheries & Wildlife Sciences. https://doi.org/10.4172/2375-446X.1000138

[21] Daâssi, D., S. Rodríguez-Couto, M. Nasri, and T. Mechichi, 2014. Biodegradation of textile dyes by immobilized laccase from Coriolopsis gallica into Ca-alginate beads. International Biodeterioration & Biodegradation, 90: 71-78. https://doi.org/10.1016/j.ibiod.2014.02.006

[22] Adegoke, K.A. and O.S. Bello, 2015. Dye sequestration using agricultural wastes as adsorbents. Water Resources and Industry, 12: 8-24. https://doi.org/10.1016/j.wri.2015.09.002

[23] El Harfi, S. and A. El Harfi, 2017. Classifications, properties and applications of textile dyes: A review. Applied Journal of Environmental Engineering Science, 3(3): 00000-3 N° 3 (2017) 311-320.

[24] Katheresan, V., J. Kansedo, and S.Y. Lau, 2018. Efficiency of various recent wastewater dye removal methods: A review. Journal of environmental chemical engineering, 6(4): 4676-4697. https://doi.org/10.1016/j.jece.2018.06.060

[25] Arslan, S., M. Eyvaz, E. Gürbulak, and E. Yüksel, 2016. A review of state-of-the-art technologies in dye-containing wastewater treatment-the textile industry case. Textile wastewater treatment: 1-29. https://doi.org/10.5772/64140

[26] Yaseen, D. and M. Scholz, 2019. Textile dye wastewater characteristics and constituents of synthetic effluents: a critical review. International journal of environmental science and technology, 16(2): 1193-1226. https://doi.org/10.1007/s13762-018-2130-z

[27] Shekofteh-Gohari, M., A. Habibi-Yangjeh, M. Abitorabi, and A. Rouhi, 2018. Magnetically separable nanocomposites based on ZnO and their applications in photocatalytic processes: a review. Critical Reviews in Environmental Science and Technology, 48(10-12): 806-857. https://doi.org/10.1080/10643389.2018.1487227

[28] Lashkenari, M.S., A. Khosravi Ghasemi, M. Ghorbani, and S. Rezaei, 2021. Fabrication of RGO/PANI-supported Pt/Cu nanoparticles as robust electrocatalyst for alkaline methanol electrooxidation. Journal of Materials Science: Materials in Electronics, 32(4): 4833-4845. https://doi.org/10.1007/s10854-020-05222-5

[29] Wang, H., X. Liu, and S. Han, 2016. The synthesis of a Ag-ZnO nanohybrid with plasmonic photocatalytic activity under visible-light irradiation: the relationship between tunable optical absorption, defect chemistry and photocatalytic activity. CrystEngComm, 18(11): 1933-1943. https://doi.org/10.1039/C5CE02381E

[30] Nidheesh, P., 2015. Heterogeneous Fenton catalysts for the abatement of organic pollutants from aqueous solution: a review. Rsc Advances, 5(51): 40552-40577. https://doi.org/10.1039/C5RA02023A

[31] Varma, R.S., 2014. Journey on greener pathways: from the use of alternate energy inputs and benign reaction media to sustainable applications of nano-catalysts in synthesis and environmental remediation. Green Chemistry, 16(4): 2027-2041. https://doi.org/10.1039/c3gc42640h

[32] Luo, L., H. Li, Y. Peng, C. Feng, and J. Zeng, 2018. Rh-based nanocatalysts for heterogeneous reactions. ChemNanoMat, 4(5): 451-466. https://doi.org/10.1002/cnma.201800033

[33] Chen, S., X. Zhang, Y. Xiang, J. Fan, and L.-Y. Gan, 2022. Computational screening of single transition metal atom embedded in nitrogen doped graphene for CH4 detection. Materials Today Communications, 31: 103383. https://doi.org/10.1016/j.mtcomm.2022.103383

[34] Hu, H., J.H. Xin, H. Hu, X. Wang, D. Miao, and Y. Liu, 2015. Synthesis and stabilization of metal nanocatalysts for reduction reactions-a review. Journal of materials chemistry A, 3(21): 11157-11182. https://doi.org/10.1039/C5TA00753D

[35] Hassanien, A.S. and A.A. Akl, 2018. Optical characteristics of iron oxide thin films prepared by spray pyrolysis technique at different substrate temperatures. Applied Physics A, 124(11): 1-16. https://doi.org/10.1007/s00339-018-2180-6

[36] Wu, W., C. Jiang, and V.A. Roy, 2015. Recent progress in magnetic iron oxide-semiconductor composite nanomaterials as promising photocatalysts. Nanoscale, 7(1): 38-58. https://doi.org/10.1039/C4NR04244A

[37] Azeredo, B., A. Carton, C. Leuvrey, C. Kiefer, D. Ihawakrim, S. Zafairatos, M. Gallart, P. Gilliot, and B.P. Pichon, 2018. Synergistic photo optical and magnetic properties of a hybrid nanocomposite consisting of a zinc oxide nanorod array decorated with iron oxide nanoparticles. Journal of Materials Chemistry C, 6(39): 10502-10512. https://doi.org/10.1039/C8TC02680G

[38] Subash, B., B. Krishnakumar, R. Velmurugan, M. Swaminathan, and M. Shanthi, 2012. Synthesis of Ce co-doped Ag-ZnO photocatalyst with excellent performance for NBB dye degradation under natural sunlight illumination. Catalysis Science & Technology, 2(11): 2319-2326. https://doi.org/10.1039/c2cy20254a

[39] Kerli, S., M. Kavgacı, A.K. Soğuksu, and B. Avar, 2022. Photocatalytic Degradation of Methylene Blue, Rhodamine-B, and Malachite Green by Ag@ ZnO/TiO2. Brazilian Journal of Physics, 52(1): 1-11. https://doi.org/10.1007/s13538-021-01007-1

[40] Kwiatkowski, M., ZnO (core)/TiO2 (shell) composites: influence of TiO2 microstructure, N-doping and decoration with Au nanoparticles on photocatalytic and photoelectrochemical activity, 2017, Bourgogne Franche-Comté.

[41] Zhao, F., Q. Lu, and S. Liu, 2014. Preparation and characterization of In2O3/ZnO heterostructured microbelts by sol-gel combined with electrospinning method. Journal of sol-gel science and technology, 69(2): 357-363. https://doi.org/10.1007/s10971-013-3225-0

[42] Eskizeybek, V., F. Sarı, H. Gülce, A. Gülce, and A. Avcı, 2012. Preparation of the new polyaniline/ZnO nanocomposite and its photocatalytic activity for degradation of methylene blue and malachite green dyes under UV and natural sun lights irradiations. Applied Catalysis B: Environmental, 119: 197-206. https://doi.org/10.1016/j.apcatb.2012.02.034

[43] Dai, K., J. Lv, L. Lu, Q. Liu, G. Zhu, and D. Li, 2014. Synthesis of micro-nano heterostructure AgBr/ZnO composite for advanced visible light photocatalysis. Materials Letters, 130: 5-8. https://doi.org/10.1016/j.matlet.2014.04.190

[44] El-Naggar, M.E., S. Shaarawy, and A. Hebeish, 2018. Multifunctional properties of cotton fabrics coated with in situ synthesis of zinc oxide nanoparticles capped with date seed extract. Carbohydrate polymers, 181: 307-316. https://doi.org/10.1016/j.carbpol.2017.10.074

[45] Talooki, E.F., M. Ghorbani, M. Rahimnejad, and M.S. Lashkenari, 2020. Evaluation of a visible light-responsive polyaniline nanofiber- cadmium sulfide quantum dots photocathode for simultaneous hexavalent chromium reduction and electricity generation in photo-microbial fuel cell. Journal of Electroanalytical Chemistry, 873: 114469. https://doi.org/10.1016/j.jelechem.2020.114469

[46] Davari, N., M. Farhadian, A.R.S. Nazar, and M. Homayoonfal, 2017. Degradation of diphenhydramine by the photocatalysts of ZnO/Fe2O3 and TiO2/Fe2O3 based on clinoptilolite: structural and operational comparison. Journal of environmental chemical engineering, 5(6): 5707-5720. https://doi.org/10.1016/j.jece.2017.10.052

[47] MacDonald, M., J. Vorberger, E. Gamboa, R. Drake, S. Glenzer, and L. Fletcher, 2016. Calculation of Debye-Scherrer diffraction patterns from highly stressed polycrystalline materials. Journal of Applied Physics, 119(21): 215902. https://doi.org/10.1063/1.4953028

[48] George, A., D.M.A. Raj, X. Venci, A.D. Raj, A.A. Irudayaraj, R. Josephine, S.J. Sundaram, A.M. Al-Mohaimeed, D.A. Al Farraj, and T.-W. Chen, 2022. Photocatalytic effect of CuO nanoparticles flower-like 3D nanostructures under visible light irradiation with the degradation of methylene blue (MB) dye for environmental application. Environmental Research, 203: 111880. https://doi.org/10.1016/j.envres.2021.111880

[49] Soleimani-Lashkenari, M., S. Rezaei, J. Fallah, and H. Rostami, 2018. Electrocatalytic performance of Pd/PANI/TiO2 nanocomposites for methanol electrooxidation

in alkaline media. Synthetic Metals, 235: 71-79. https://doi.org/10.1016/j.synthmet.2017.12.001

[50] Khurshid, F., M. Jeyavelan, M.S.L. Hudson, and S. Nagarajan, 2019. Ag-doped ZnO nanorods embedded reduced graphene oxide nanocomposite for photo-electrochemical applications. Royal Society open science, 6(2): 181764. https://doi.org/10.1098/rsos.181764

[51] Qin, J., X. Zhang, C. Yang, M. Cao, M. Ma, and R. Liu, 2017. ZnO microspheres-reduced graphene oxide nanocomposite for photocatalytic degradation of methylene blue dye. Applied Surface Science, 392: 196-203. https://doi.org/10.1016/j.apsusc.2016.09.043

[52] Lashkenari, M.S., M. Ghorbani, N. Silakhori, and H. Karimi-Maleh, 2021. Enhanced electrochemical performance and stability of Pt/Ni electrocatalyst supported on SiO2-PANI nanocomposite: a combined experimental and theoretical study. Materials Chemistry and Physics, 262: 124290. https://doi.org/10.1016/j.matchemphys.2021.124290

[53] Dargahi, Z., H. Asgharzadeh, and H. Maleki-Ghaleh, 2018. Synthesis of Mo-doped TiO2/reduced graphene oxide nanocomposite for photoelectrocatalytic applications. Ceramics International, 44(11): 13015-13023. https://doi.org/10.1016/j.ceramint.2018.04.120